High-β equilibria in tokamaks with toroidal flow

Michael Fitzgerald, Sergei Sharapov, and Matthew Hole

Citation: Phys. Plasmas **18**, 092508 (2011); doi: 10.1063/1.3641966
View online: http://dx.doi.org/10.1063/1.3641966
View Table of Contents: http://pop.aip.org/resource/1/PHPAEN/v18/i9
Published by the American Institute of Physics.

High-β equilibria in tokamaks with toroidal flow

Michael Fitzgerald,[1,a)] Sergei Sharapov,[2] and Matthew Hole[1]
[1]*Research School of Physical Sciences and Engineering, Australian National University, 0200 ACT, Australia*
[2]*EURATOM/CCFE Fusion Association, Culham Science Centre, Abingdon, Oxfordshire OX14 3DB, United Kingdom*

(Received 5 June 2011; accepted 24 August 2011; published online 29 September 2011)

We extend existing 2-D analytical high-β equilibrium solutions obtained by Cowley *et al.* [Phys. Fluids B **3**, 2066 (1991)] and Hsu *et al.* [Phys. Plasmas **3**, 266 (1996)] to the case of toroidally flowing plasma, assuming ideal magnetohydrodynamics and isothermal magnetic surfaces. Invoking the ordering $\beta q^2 \gg \epsilon^2$ and $M_\phi^2 q^2 \gg \epsilon$, we solve the boundary layer problem, re-obtaining the static solution in the zero flow limit. The phenomenon of extreme plasma diamagnetism in the static solution was found to be reduced due to centrifugal drift currents for significant toroidal flow. Example equilibrium calculations are presented using plasma parameters which are approaching attainable values in next generation spherical tokamaks. © *2011 American Institute of Physics*.
[doi:10.1063/1.3641966]

I. INTRODUCTION

To operate and understand a modern, high performance tokamak, one requires a good model for the magnetohydrodynamic (MHD) force balance. The success of the spherical tokamak concept makes new demands of the equilibrium theory, such as requiring models which include inverse aspect ratio $\epsilon = a/R_0$ order unity and significant toroidal flows or pressure anisotropy.[1] Good MHD stability allows for the ratio $\beta = 2\mu_0 p/B^2$ to increase and approach unity.[2] This has been experimentally verified on START[3] and NSTX[4] in discharges with volume averaged toroidal beta ($\beta_T \equiv 2\mu_0\langle p\rangle/B_{T0}^2$) of 40%. The proposed Component Test Facility (CTF) and Spherical Tokamak Power Plant (STPP) concepts[5,6] are projected to achieve volume averaged toroidal betas of 30% and 60%, respectively, with significant plasma flows in the former resulting from tangentially oriented Neutral Beam Injection (NBI) heating.

Analytical solutions of the high-β MHD equilibrium exist in 2-D symmetric toroidal geometry for small[7] and unity[8] inverse aspect ratio limits. These solutions exhibit a large Shafranov shift of the magnetic axis separating the solution into a predominantly 1-D "core" region and a thin "boundary layer" solution (Fig. 1). For sufficiently high pressure, plasma diamagnetism becomes important, causing the magnetic field to be expelled from the magnetic axis region for the more extreme cases. The MHD equilibrium equations have been generalised by various authors[9–11] to include the centrifugal forces of a rotating plasma. The addition of a centrifugal force will, for large flows, displace the pressure surfaces from magnetic surfaces. The Grad-Shafranov equation used for static solutions can be generalised by introducing a Bernoulli equation for energy conservation and an assumption about heat flow.

This paper generalises the previous high-β MHD solutions by including the effect of toroidal flows in the limit of isothermal flux surfaces.

a)Electronic mail: Michael.Fitzgerald@anu.edu.au.

II. EQUILIBRIUM WITH TOROIDAL FLOW

Here, we summarize the derivation of the Grad-Shafranov equation for purely toroidal flow that has been presented elsewhere[12–15] but in sporadic detail for the isothermal assumption $\vec{B}\cdot\nabla T = 0$. This paper deals with the 2-D cylindrically symmetric system in Fig. 2. We begin with the fundamental result that divergence-free quantities in 2-D axisymmetric systems can be expressed in terms of poloidal flux functions ψ and ψ_M for magnetic field and momentum, respectively,

$$\vec{B} = \nabla\psi \times \nabla\phi + F\nabla\phi, \tag{1}$$

$$\rho\vec{u} = \nabla\psi_M \times \nabla\phi + F_M\nabla\phi, \tag{2}$$

where $F(R,Z)$ and $F_M(R,Z)$ are arbitrary. In this paper, we make the ideal MHD assumption with zero resistivity,

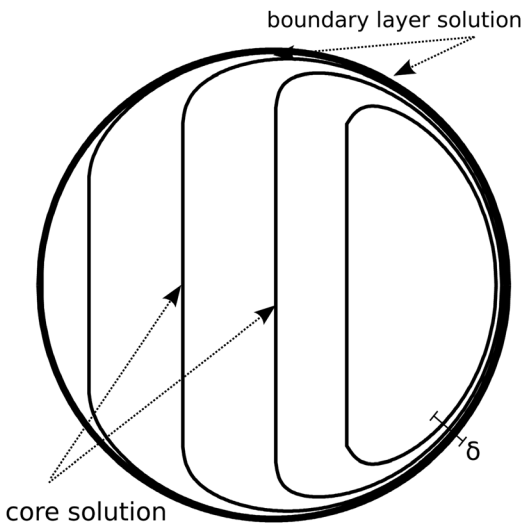

FIG. 1. Illustration depicting contours of constant poloidal magnetic flux ψ given by the high-β analytical solution. The core and boundary regions are solved separately.

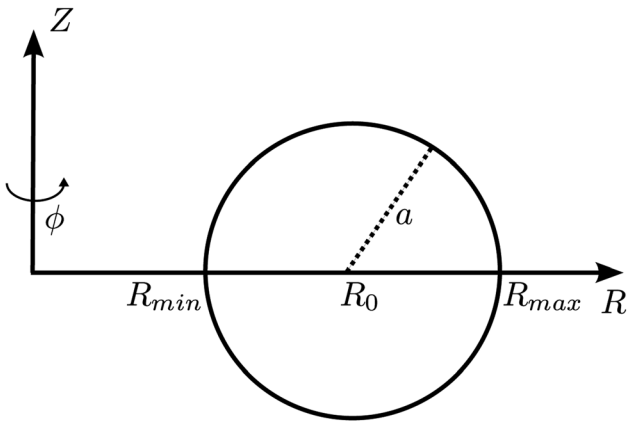

FIG. 2. Cylindrical coordinate system and relevant geometric parameters. The circle represents the plasma boundary.

$$\vec{E} + \vec{u} \times \vec{B} = 0, \tag{3}$$

we then obtain magnetic field lines which are "frozen" into the plasma. For a 2-D flowing plasma, the plasma can only move along the field lines or by the rigid rotation of field and plasma in the symmetry direction $\hat{\phi}$. One can substitute momentum flux and Faraday's law into Eq. (3) to obtain the well known 2-D axis-symmetric result for the velocity,

$$\vec{u} = \frac{\psi_M(\psi)}{\rho}\vec{B} + \Omega(\psi)R\hat{\phi}, \tag{4}$$

which expresses the frozen-in condition. It is interesting to note that under these assumptions, a purely poloidal flow is not possible unless the toroidal field is zero.

Turning now to the momentum equation,

$$\rho\vec{u} \cdot \nabla\vec{u} = -\nabla p + \vec{J} \times \vec{B}, \tag{5}$$

we wish to simplify the problem by using a thermodynamic state function which relates ρ, ∇T, and ∇p so that the chosen independant variables are clear. The natural choice for the isothermal case is the Gibbs free energy $G(T, p)$,

$$\nabla G = -S\nabla T + V\nabla p, \tag{6}$$

where we neglect other energy losses from the system (e.g., $dN = 0$). Using the result $u_\phi = \Omega\,(\psi)R$, we may write

$$-\rho\left(\frac{1}{2}\nabla\left(R^2\Omega^2\right) + R^2\Omega\Omega'\nabla\psi\right) + \frac{\nabla G}{V} + \frac{S}{V}\nabla T = \vec{J} \times \vec{B}. \tag{7}$$

Taking the dot product with $\vec{B}$ terms in $\nabla\psi$ and ∇T are zero and we obtain a new flux function,

$$H(\psi) = -\frac{1}{2}R^2\Omega^2 + \frac{G}{mN}, \tag{8}$$

this is the Bernoulli equation for energy conservation along a fluid stream line. Substituting this new flux function H to eliminate G from our fluid equation we obtain

$$-\rho R^2\Omega\Omega'\nabla\psi + \rho\nabla H + \frac{S}{V}\nabla T = \vec{J} \times \vec{B}, \tag{9}$$

which has all components parallel to $\nabla\psi$ and a scalar equation for the components as in the Grad-Shafranov equation (see, for example, the text by Bellan[16]). We can eliminate the entropy S from the equation by specifying[12] G,

$$G = NkT\log\frac{\rho}{\rho_0}, \tag{10}$$

$$S = -\left(\frac{\partial G}{\partial T}\right)_p = -Nk\log\frac{\rho}{\rho_0} + Nk, \tag{11}$$

for any arbitrary reference ρ_0. In the absence of toroidal forces, F is constrained to be $F = F(\psi)$ and we use the result (in natural units for convenience),

$$\vec{J} \times \vec{B} = -\left[\frac{FF'}{R^2} + \nabla \cdot \left(\frac{\nabla\psi}{R^2}\right)\right]\nabla\psi, \tag{12}$$

and obtain a Grad-Shafranov equation,

$$R^2\nabla \cdot \left(\frac{\nabla\psi}{R^2}\right) = -FF' - R^2\rho H' - R^2\frac{k}{m}\left(\rho - \rho\log\frac{\rho}{\rho_0}\right)T' + \rho R^4\Omega\Omega', \tag{13}$$

where the left hand side is often written $\Delta^*\psi$.

An important result from our Bernoulli relation (Eq. (8)) is that we may express the mass density as

$$\rho(R,\psi) = \bar{K}(\psi)\exp\left(\frac{m\Omega^2(\psi)R^2}{2kT(\psi)}\right), \tag{14}$$

where $\bar{K}(\psi) \equiv \rho_0\exp(mH(\psi)/kT(\psi))$. This expresses the centrifugal shift of the density away from flux surfaces and is clearly just an expression of the Boltzmann distribution in the presence of a centrifugal force.

III. QUALITATIVE PICTURE

Before giving the complete solution, we can deduce properties of the solution by examining the force balance equations.

A. Ordering

We consider the fluid equation (in natural units),

$$\rho\vec{u} \cdot \nabla\vec{u} = -\nabla p + \vec{J} \times \vec{B} = -\nabla p - \frac{\nabla B_\phi^2}{2} - \frac{\nabla B_\theta^2}{2} - B_\phi^2\frac{\nabla R}{R} + \vec{B_\theta} \cdot \nabla\vec{B_\theta}, \tag{15}$$

where $\vec{B_\theta}$ denotes the poloidal field $\nabla\psi \times \nabla\phi$ and B_ϕ denotes the toroidal field $F\nabla\psi$. For the sake of order-of-magnitude approximation, we assume the forms,

$$q \approx \frac{rB_\phi}{RB_\theta} = O\left(\epsilon\frac{B_\phi}{B_\theta}\right), \tag{16}$$

$$\rho\vec{u} \cdot \nabla\vec{u} = \rho\vec{u_\phi} \cdot \nabla\vec{u_\phi} = -\rho u_\phi^2\frac{\nabla R}{R} = O\left(\epsilon\rho u_\phi^2\right), \tag{17}$$

$$\beta = \frac{2p}{B^2} = O\left(\frac{p}{B_\phi^2}\right), \tag{18}$$

$$\rho u_\phi^2 = M_\phi^2 B_\phi^2, \tag{19}$$

where M_ϕ is the toroidal Alvén Mach Number, u_ϕ is the toroidal velocity, and q is the tokamak safety factor. We can now order the equation against B_ϕ^2 with dimensionless quantities,

$$\underbrace{\rho\vec{u}\cdot\nabla\vec{u}}_{O\left(\epsilon M_\phi^2\right)} = \underbrace{-\nabla p}_{O(\beta)} \underbrace{-\frac{\nabla B_\phi^2}{2}}_{O(1)} \underbrace{-\frac{\nabla B_\theta^2}{2}}_{O\left(\frac{\epsilon^2}{q^2}\right)} \underbrace{-B_\phi^2\frac{\nabla R}{R}}_{O(\epsilon)} \underbrace{+\vec{B}_\theta\cdot\nabla\vec{B}_\theta}_{O\left(\frac{\epsilon^2}{q^2}\right)}. \tag{20}$$

We specify that for ''high-β'' solutions we mean that $\beta q^2 \gg \epsilon^2$. If $\beta \gg \epsilon M_\phi^2$, then toroidal flow effects are not significant for these high-β solutions and we regain the previous static results.[7,8]

B. Core and boundary solutions

We are concerned with the core region where $M_\phi^2 q^2 \gg \epsilon$ and $\beta q^2 \gg \epsilon^2$. In this case

$$\rho\vec{u}\cdot\nabla\vec{u} = -\nabla p - \frac{\nabla B_\phi^2}{2} - B_\phi^2\frac{\nabla R}{R}. \tag{21}$$

Exploiting previous results for toroidal rotation,

$$u_\phi(R,\psi) = \Omega(\psi)R \tag{22}$$

$$\rho(R,\psi) = \bar{K}(\psi)\exp\left(\frac{m\Omega^2(\psi)R^2}{2kT(\psi)}\right), \tag{23}$$

$$p(R,\psi) = \frac{\rho(R,\psi)}{m}kT(\psi), \tag{24}$$

$$B_\phi(R,\psi) = \frac{F(\psi)}{R}. \tag{25}$$

We can re-write the components of Eq. (21) as

$$\begin{aligned}
\vec{u_\phi}\cdot\nabla\vec{u_\phi} &= \frac{-u_\phi^2}{R}\nabla R = -R\Omega^2(\psi)\nabla R\\
\nabla p(R,\psi) &\equiv \alpha_1(R,\psi)\nabla\psi + \alpha_2(R,\psi)\nabla R\\
\frac{\nabla B_\phi^2(R,\psi)}{2} &\equiv \alpha_3(R,\psi)\nabla\psi + \alpha_4(R,\psi)\nabla R\\
\rho R\Omega^2\nabla R &= \alpha_1\nabla\psi + \alpha_2\nabla R\\
&\quad + \alpha_3\nabla\psi + \alpha_4\nabla R + B_\phi^2\frac{\nabla R}{R},
\end{aligned} \tag{26}$$

where α's are scalars. It follows that ∇R and $\nabla\psi$ are parallel which further implies that $\psi = \psi(R)$ in the core.

The assumption that flux surfaces must close implies the existence of a boundary region outside the core where poloidal field terms are important. The better the core approximation represents the system, the smaller the boundary solution region will be. This boundary layer can be characterised by a width δ (Fig. 1) such that the magnitude of the poloidal field $|\nabla\psi|/r$ is a/δ times larger in the boundary layer than in the core. The size of the boundary layer can be deduced from the unbalanced pressure and centrifugal forces, the larger of which we expect to be the pressure term. The previous studies on static equilibria[7,8] quote a first order unbalanced pressure of ∇ leading to $\delta/a \approx O(\sqrt{\epsilon/\beta q^2})$.

IV. SOLUTION

We proceed by solving the Grad-Shafranov equation (Eq. (13)) for the two asymptotic regions separately.

A. Core solution

Taking the limit $Bq^2 \gg \epsilon^2$ for the core region, the Grad-Shafranov operator $\Delta^*\psi$ becomes zero,

$$0 = -FF' - R^2\rho H' - R^2\frac{k}{m}\left(\rho - \rho\log\frac{\rho}{\rho_0}\right)T' + \rho R^4\Omega\Omega'. \tag{27}$$

To simplify the solution, we introduce a new spatial variable $X(\psi)$ much in the same way as a previous work;[8] however, we must take greater care to eliminate all R dependence from the equation than in the static solution, or else the usefulness of this particular approach is lost. We define $X(\psi)$ implicitly with

$$\begin{aligned}
0 \equiv{}& -F(X)F'(X) - X^2\rho_c H'(X)\\
&- X^2\frac{k}{m}\left(\rho_c - \rho_c\log\frac{\rho_c}{\rho_0}\right)T'(X) + \rho X^4\Omega(X)\Omega'(X),
\end{aligned} \tag{28}$$

$$\rho_c(X) \equiv \bar{K}(X)\exp\left(\frac{m\Omega^2(X)X^2}{2kT(X)}\right), \tag{29}$$

where we have also defined a new mass density ρ_c. Comparing Eqs. (28) and (27), we see that $R = X(\psi)$ in the core by construction. Therefore, $\rho_c(X)$ is equal to the value of the density as a function of R in the core. Observe also that in introducing $X(\psi)$ we have replaced the free poloidal flux functions with new free functions of X: $\Omega(X)$, $T(X)$, $H(X)$, and $F(X)$.

For the rest of the paper, it will be useful to label the right-hand side of our Grad-Shafranov equation in terms of the toroidal current density J_ϕ and eliminate ψ,

$$\rho(R,X) = \rho_c(X)\exp\left(\frac{m\Omega^2(X)(R^2 - X^2)}{2kT(X)}\right), \tag{30}$$

$$\begin{aligned}
RJ_\phi(R,X) \equiv{}& -FF' - R^2\rho H'\\
&- R^2\frac{k}{m}\left(\rho - \rho\log\frac{\rho}{\rho_0}\right)T' + \rho R^4\Omega\Omega',
\end{aligned} \tag{31}$$

$$\begin{aligned}
XJc_\phi(X) \equiv{}& -FF' - X^2\rho_c H'\\
&- X^2\frac{k}{m}\left(\rho_c - \rho_c\log\frac{\rho_c}{\rho_0}\right)T' + \rho_c X^4\Omega\Omega',
\end{aligned} \tag{32}$$

and we also henceforth return to S.I. units using the dimensionally correct transformation,[17]

$$\psi \to \frac{\psi}{\sqrt{\mu_0}}, F \to \frac{F}{\sqrt{\mu_0}}, B \to \frac{B}{\sqrt{\mu_0}}, J \to J\sqrt{\mu_0}. \tag{33}$$

B. Boundary layer solution

Outside of the core region, the poloidal field terms become significant, and we express our Grad-Shafranov equation in terms of distance from the boundary ξ,

$$\frac{d^2\psi}{d\xi^2}(R,X) = \mu_0(RJ_\phi(R,X) - XJc_\phi(X)). \tag{34}$$

Rewriting the second order derivative as

$$\frac{d^2\psi}{d\xi^2} = \frac{1}{2(\partial\psi/\partial\xi)}\frac{\partial}{\partial\xi}\left[\left(\frac{\partial\psi}{\partial\xi}\right)^2\right], \tag{35}$$

we integrate once and obtain

$$\left(\frac{\partial\psi}{\partial\xi}\right)^2 = 2\mu_0\int(RJ_\phi(R,X) - XJc_\phi(X))\frac{\partial\psi}{\partial\xi}d\xi, \tag{36}$$

we wish to change variables from ψ to X. We expect a rapid variation of ψ over a thin boundary layer, which implies that R is independent of ψ in the integral. This allows us to write (to first order)

$$\left(\frac{\partial\psi}{\partial\xi}(R,X)\right)^2 = 2\mu_0\int_R^X(RJ_\phi(R,X'') - X''Jc_\phi(X''))dX'', \tag{37}$$

with the prime denoting the dummy integration variable in this context. Given that $B_\theta = \nabla\psi \times \nabla\phi$, we see that Eq. (37) gives the poloidal field in the boundary layer because $(\partial_\xi\psi)^2 = R^2B_\theta^2$. Integrating again, we arrive at the solution for the boundary layer,

$$\xi(R,X) = \int_{R_{min}}^X \frac{\frac{d\psi}{dX'}dX'}{\sqrt{2\mu_0\int_R^{X'}(RJ_\phi(R,X'') - X''Jc_\phi(X''))dX''}}, \tag{38}$$

where R_{min} is taken as location of the inboard side along the major axis. As in Hsu *et al.*,[8] we have chosen our integration limits so that $R \to X$ as we approach the core solution from the boundary. Note that $R \geq X$ for all physical solutions.

C. Computing the solution

We may now collect the elements of the solution into a complete description. To construct the solution, we start by specifying the input functions of X. A convenient set of functions are $T(X)$, $\rho_c(X)$, $\Omega(X)$, and $\partial\psi/\partial X(X)$. Unlike poloidal flux functions, these profiles could be directly measured by taking measurements in the core as functions of R (and using $d\psi/dX = XB_\theta$). This asymptotic approximation may be improved for finite boundary layer width by scaling X to have a maximum at the magnetic axis instead of the wall.

Once the input functions have been specified, the equilibrium is obtained by drawing contours of constant X in the core and boundary layer and joining the solutions. The lines of constant X in the core are simply vertical lines of constant R. The lines of constant X in the boundary are found by tracing a perpendicular distance $\xi(R,X)$ from the wall at any given R value. For smooth joining of the contours, numerical points should be concentrated around the $R \to X$ transition where $\xi(R, X)$ varies rapidly.

For completeness, we give explicit expressions for q and $\vec{B}$. Taking first the general expression of q,

$$q(\psi) = \frac{F(\psi)}{2\pi}\oint\frac{dl}{R|\nabla\psi|}, \tag{39}$$

where the line integral is performed on a loop of constant ψ. In the boundary layer portion of the loop, we expect $\nabla\psi$ to be large and the integrand to be small. To first order, the expression for q reduces to a line integral along the vertical contours in the core, giving

$$q(X) = \frac{F(X)}{2\pi X}\frac{l(X)}{|d\psi/dX|}, \tag{40}$$

where $l(X)$ is the length of the vertical line from top boundary layer to bottom boundary layer. In the limit of small boundary layer, this is simply the vertical height of the plasma boundary.

Our expressions for the magnetic field come directly from Eq. (1). The toroidal field is given by

$$\vec{B_\phi} = \frac{F(X)}{R}\hat{\phi}. \tag{41}$$

The poloidal fields in the core and boundary layer, respectively, are given by

$$\vec{B_\theta} = \frac{|d\psi/dX|}{X}\widehat{\nabla X \times \phi}, \tag{42}$$

$$\vec{B_\theta} = \frac{|d\psi/d\xi|}{R}\widehat{\nabla X \times \phi}. \tag{43}$$

D. Joining the solutions and self-consistency

By using the matching condition $d\psi/d\xi \to 0$ as $R \to X$, we have introduced a discontinuity in the derivative of the flux function at the border between the core and boundary solutions. The dotted lines in Fig. 3 represent tangents to the boundary layer solution at the border. Each tangent is parallel with ξ consistent with $d\psi/d\xi \to 0$. Because Z and ξ are generally not parallel at the border, the derivatives $d\psi/dZ$ and $d\psi/d\xi$ are equal if and only if $d\psi/dR \to 0$. This mismatch of derivatives causes a fictitious surface current at the border which corresponds to a disagreement between B_θ either side of the border. Equations (42) and (43) give the measured value of B_θ in the core and the calculated value of B_θ in the boundary layer, respectively. The magnitude of the fictitious surface current density $|\vec{K}|$ is given by

$$|\vec{K}| = \frac{|d\psi/dX|}{X}. \tag{44}$$

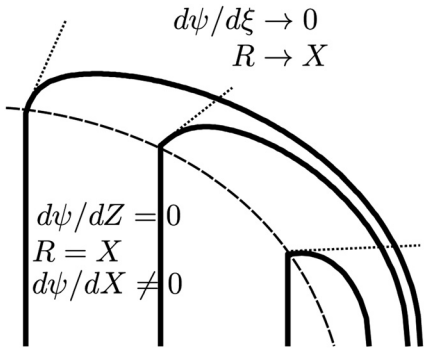

FIG. 3. Illustration of the border between the core and boundary layer solutions. A dashed line denotes the surface bordering the two regions. The dotted lines are tangents to the boundary layer solution which make the discontinuity in derivative across the border more obvious.

Unphysical current gradients could lead to the appearance of artificial instabilities such as tearing modes which work to smooth the discontinuous gradient. Thus, for well behaved analytical solutions, we should use Eq. (43) for the whole solution so that $B_\theta \to 0$ smoothly to the core. Since $\nabla\psi$ is never computed directly to find B_θ, the discontinuity in derivative is never encountered. Ultimately, this requirement is a consequence of our approximation $\beta q^2 \gg \epsilon^2$ that B_θ terms are unimportant in the core region.

V. PLASMA DIAMAGNETISM WITH FLOW

As we have not nominated $F(X)$ as a free function, we must find an expression for $F(X)$ in terms of our free functions to enable calculation of the toroidal field. We rearrange the definition of X in Eq. (28) and obtain

$$F(X) = \sqrt{F(R_{min})^2 - 2\mu_0 \int_{R_{min}}^{X} \mathcal{D}(X')dX'}, \tag{45}$$

$$\mathcal{D}(X) \equiv [X^2\rho_c H' + X^2\frac{k}{m}\left(\rho_c - \rho_c \log\frac{\rho_c}{\rho_0}\right)T' - X^4\rho_c\Omega\Omega'], \tag{46}$$

it is useful here to introduce the pressure in the core $p_c(X) = (\rho_c(X)/m)kT(X)$. Eq. (46) becomes

$$\mathcal{D}(X) \equiv \left[X^2 p'_c - X^3\rho_c\Omega^2 - 2X^4\rho_c\Omega\Omega'\right]. \tag{47}$$

Equation (45) gives an expression for the poloidal current responsible for the toroidal field. The integral represents plasma contributions to the poloidal current. A similar expression has been derived previously for the static case[7,8] which can be regained exactly by setting $\Omega = 0$ in Eq. (47).

Under circumstances where the integral term in Eq. (45) approaches or exceeds $F(R_{min})^2$, a region of perfect diamagnetism exists and there are no physical solutions of the Grad-Shafranov equation. We must therefore restrict our Grad-Shafranov solution domain for X to regions outside of the "diamagnetic hole." Within the hole, one should start with a field free fluid equation and solve the ordinary hydrodynamics problem.

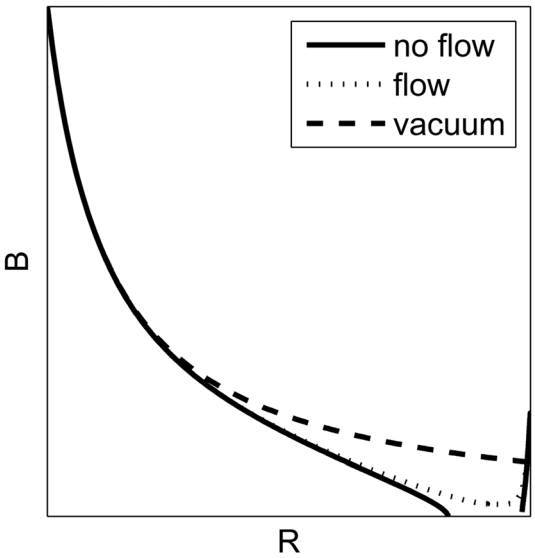

FIG. 4. Illustration of a typical MHD hole solution. Plasma diamagnetism in high-β solutions can decrease the vacuum field to zero. Toroidal rotation can reverse this effect.

An interesting feature of the flow solution is the suppression of plasma diamagnetism by rotation. Fig. 4 shows the typical affect of plasma pressure and rotation on the total field for large β and Ω (specific values in the calculation will be discussed in Sec. VI). In regions far from the magnetic axis, the plasma pressure and rotation tend to be smaller and have little effect on the magnetic field in comparison to the vacuum solution. The diamagnetic hole appears in the region of highest pressure. As rotation is increased, the size of the hole region is reduced and may be eliminated entirely as in Fig. 4. This effect will be strongest when the rotation is fast near the magnetic axis, which is often the case.

We may understand rotation suppression of diamagnetism in terms of drift currents. Consider the fluid equation for a slowly varying plasma which rotates in the toroidal direction. Separating the currents and fields into free and magnetisation contributions $\vec{B} \equiv \vec{M} + \vec{H}$ and setting the time derivative to zero

$$-\rho\frac{u^2}{r}\hat{r} = (\vec{J}_M + \vec{J}_{free}) \times (\vec{M} + \vec{H}) - \nabla p, \tag{48}$$

we are free to set the external field H and current J_{free} to zero and look at plasma contributions to the current with

$$-\rho\frac{u^2}{r}\hat{r} = \vec{J}_M \times \vec{M} - \nabla p, \tag{49}$$

taking the cross product with the field, we obtain the perpendicular dynamics

$$\vec{J}_M = -\frac{\nabla p \times \vec{M}}{M^2} + \frac{\rho R\Omega^2\hat{r} \times \vec{M}}{2M^2}. \tag{50}$$

The first term on the right hand side of Eq. (50) is the familiar diamagnetic current. The second term contains the drift current arising from inertial forces which is a well known prediction of the single-particle drift equations. We see that

the total plasma current is the sum of diamagnetic and inertial drift currents.

VI. COMPUTED EXAMPLES

We have computed some example equilibria numerically using the boundary layer solution described in Sec. IV. The free functions $T(X)$, $\Omega(X)$, $\rho_c(X)$ were taken to be of the form,

$$f(X) = f_0\left(1 - \frac{(R_{max} - X)^2}{(R_{max} - R_{min})^2}\right), \tag{51}$$

for given input $f_0 = T_0$, Ω_0, ρ_{c0}. The function $d\psi/dX$ was taken to be of the form,

$$\frac{d\psi}{dX} = a_\psi l(X), \tag{52}$$

for a given input a_ψ and circular boundary,

$$l(X) = 2\sqrt{(X - R_{min})(R_{max} - X)}. \tag{53}$$

Two example cases will be presented here: one solution including flow and one without flow. The input values used for these particular cases are given in Table I with the fluid particle mass m set to the mass of deuterium. The average toroidal beta $\beta_T \equiv 2\mu_0\langle p\rangle/B_{T0}^2$ is 60%, where $\langle p\rangle$ is the volume-average pressure and B_{T0} is the vacuum toroidal field at the geometric axis. We deliberately choose this lower β example to be closer to currently conceivable experiments (see, for example, Wilson *et al.*[5]) rather than to give the best approximation. The qualitative behaviour of higher β solutions is the same.

The computed flux surfaces for the static case ($\Omega_0 = 0$) are given in Fig. 5. The core solution where $\psi = \psi\ (R)$ is clearly distinguishable from the boundary solution. The value of ψ on each $X(\psi)$ surface may be calculated by measuring the R location of each surface in the core and then integrating $d\psi/dX$ from R_{min}.

The core and boundary solutions approach each other smoothly for regions far from the magnetic axis. The shaded region denotes where a diamagnetic hole has formed. In regions close to the transition from boundary to core solutions, where ξ is varying rapidly, a sharp transition between core and boundary is evident in Fig. 5. Profiles as a function

TABLE I. Input parameter values for the example equilibria presented in this section.

Parameter	Value
R_{min}	0.1 m
R_{max}	1 m
ρ_{c0}	$m \times 3 \times 10^{20}$ m^{-3}
kT_0	10 keV
a_ψ	0.05 T
Ω_0	0.6×10^6 s^{-1} (flow case only)
B_T at R_{min}	6 T

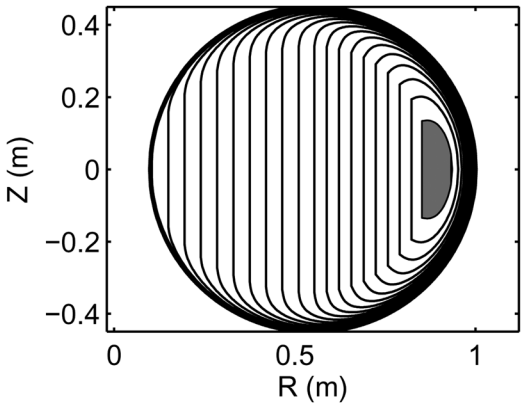

FIG. 5. Contours of constant $X(\psi)$ calculated using the values in Table I with zero flow. The shaded area denotes a magnetic field free region.

of major radius are given in Fig. 6. The large Shafranov shift causes an asymmetry in the profiles with the magnetic axis located near R_{max}. The magnetic field vanishes in this region. The $q = 1$ surface appears at $R = 0.8$ and $R = 0.96$ and borders a region of very high-β as the field vanishes, so we could expect from the linear stability theory to have a strongly driven $n = 1$ kink mode manifesting as sawtooth oscillations or even a disruption. Figs. 7 and 8 are the results of the same calculation repeated with a flow of $\Omega_0 = 0.6 \times 10^6$ s^{-1} which is approximately 600 kms^{-1}. A distortion of the density profile in Fig. 8 by centrifugal forces has produced a corresponding distortion in the pressure profile. We may note a discontinuity in the density profile on axis which results from the large value of ξ for this relatively low-β example. As the boundary thickness ξ approaches the radius of curvature of the plasma boundary, the high-β solution becomes less appropriate. This is a re-statement of the validity criterion from the previous static solutions that $\delta/a = O(\sqrt{\epsilon/\beta q^2})$ should be small.[7,8] We may remedy this by either increasing β and the Shafranov shift or using a flatter input density profile.

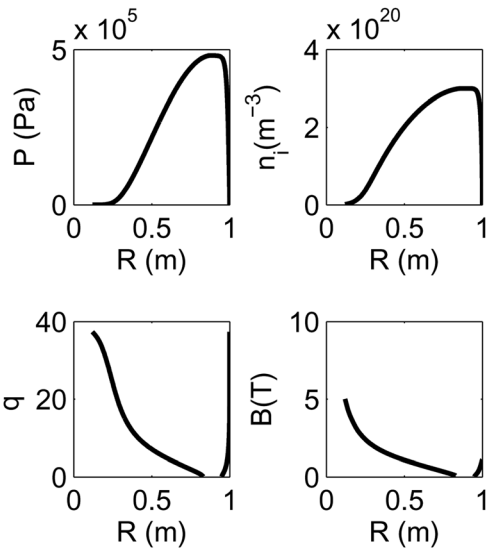

FIG. 6. Profiles as functions of major radius calculated using the values in Table I with zero flow.

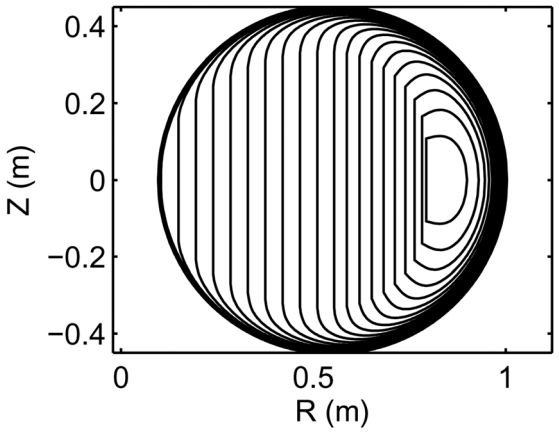

FIG. 7. Contours of constant $X(\psi)$ calculated using the values in Table I with finite flow. The finite boundary layer width at this low β produces erroneous bunching of contours near the magnetic axis.

A physical feature in the density is the prominent peak on the outboard side caused by the exponential dependence on the rotation velocity (Eq. (14)). The effects of rotation on the magnetic configuration are also apparent in Fig. 8 with the complete suppression of the diamagnetic hole. One can expect a general improvement in stability with a higher q on axis $q_0 = q(X = R_{max}) = 1.3$ and finite β.

VII. CONCLUSION

We have presented an extension to 2-D analytical high-β equilibrium solutions for toroidally flowing plasma using results from ideal MHD. In addition to assuming the ideal Ohm's law, we have also assumed isotropic thermal equilibrium along poloidal flux surfaces. These assumptions led to a Grad-Shafranov equation and Bernoulli equation for density (momentum and energy conservation, respectively). Invoking the ordering $\beta q^2 \gg \epsilon^2$ and $M_\phi^2 q^2 \gg \epsilon$, we found that $\psi = \psi\ (R)$; a result for toroidally flowing equilibrium which was the same as for static equilibrium. A boundary layer technique used previously for the static case was applied to the flow equations and an asymptotic solution was found. The phenomenon of plasma diamagnetism in the static solution was found to be reduced due to centrifugal drift currents. Example, equilibria were calculated using plasma parameters which are approaching attainable values in next generation spherical tokamaks.[5,6] These examples also demonstrated that a criterion for solution validity is that the radius of curvature of the plasma boundary must be large compared to the boundary layer thickness.

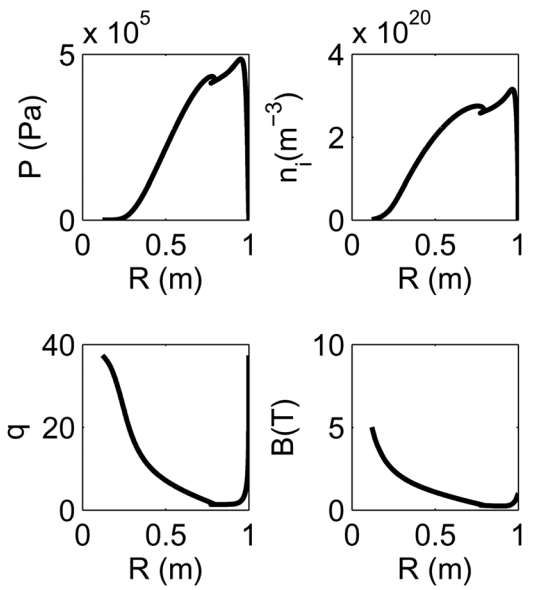

FIG. 8. Profiles as functions of major radius calculated using the values in Table I with finite flow. The diamagnetic hole from the static solution has disappeared. A centrifugal shift of the density has occurred. The bunching of contours in Fig. 7 has produced a spurious discontinuity near the magnetic axis which is absent for higher β solutions.

The physics of these high-β solutions poses interesting challenges to intuition, particularly when considering a field free region at the magnetic axis of the plasma. What are the implications of a Lamour radius which compares with the vessel dimensions when the low field region has been Shafranov-shifted to be close to the boundary? Solutions exist where ∇B can be very large in the boundary layer, what happens when the ∇B current drift in the boundary becomes the largest current in the MHD force balance? We have discovered that centrifugal forces can suppress the magnetic hole solutions, it may be interesting now to investigate whether diamagnetic holes are favourable for tokamak performance.

ACKNOWLEDGMENTS

The first author would like to acknowledge very useful discussions with Ken McClements of the Culham Centre for Fusion Energy and Ian Abel of The University of Oxford.

This work was funded by the Australian Research Council through Grant Nos. DP1093797 and FT0991899 and by the RCUK Energy Programme under Grant No. EP/I501045 and the European Communities under the contract of Association between EURATOM and CCFE. The views and opinions expressed herein do not necessarily reflect those of the European Commission.

[1]M. J. Hole, G. von Nessi, M. Fitzgerald, K. G. McClements, and J. Svensson, Plasma Phys. Controlled Fusion **53**, 074021 (2011).
[2]Y. Peng and D. Strickler, Nucl. Fusion **26**, 769 (1986).
[3]M. Gryaznevich, R. Akers, P. Carolan, N. Conway, D. Gates, A. Field, T. Hender, I. Jenkins, R. Martin, M. Nightingale, C. Ribeiro, D. Robinson, A. Sykes, M. Tournianski, M. Valovic, and M. Walsh, Phys. Rev. Lett. **80**, 3972 (1998).
[4]D. A. Gates, Phys. Plasmas **10**, 1659 (2003).
[5]H. Wilson, J.-W. Ahn, R. Akers, D. Applegate, R. Cairns, J. Christiansen, J. Connor, G. Counsell, A. Dnestrovskij, W. Dorland, M. Hole, N. Joiner, A. Kirk, P. Knight, C. Lashmore-Davies, K. McClements, D. McGregor, M. O'Brien, C. Roach, S. Tsaun, and G. Voss, Nucl. Fusion **44**, 917 (2004).
[6]Y.-K. M. Peng, P. J. Fogarty, T. W. Burgess, D. J. Strickler, B. E. Nelson, J. Tsai, C. A. Neumeyer, R. Bell, C. Kessel, J. Menard, D. Gates, B. LeBlanc, D. Mikkelsen, E. Fredrickson, L. Grisham, J. Schmidt, P. Rutherford, S. Sabbagh, A. Field, A. Sykes, I. Cook, O. Mitarai, and Y. Takase, Plasma Phys. Controlled Fusion **47**, B263 (2005).
[7]S. C. Cowley, P. K. Kaw, R. S. Kelly, and R. M. Kulsrud, Phys. Fluids B **3**, 2066 (1991).
[8]S. C. Hsu, M. Artun, and S. C. Cowley, Phys. Plasmas **3**, 266 (1996).

[9]D. Dobrott and J. Greene, Phys. Fluids **13**, 2391 (1970).
[10]H. Zehrfeld and B. Green, Nucl. Fusion **12**, 569 (1972).
[11]E. K. Maschke and H. Perrin, Plasma Phys. **22**, 579 (1980).
[12]R. Lovelace, C. Mehanian, C. Mobarry, and M. Sulkanen, Astrophys. J. Suppl. Ser. **62**, 1 (1986).
[13]A. Thyagaraja and K. G. McClements, Phys. Plasmas **13**, 062502 (2006).
[14]E. Hameiri, Phys. Fluids **26**, 230 (1983).
[15]S. Semenzato, R. Gruber, and H. Zehrfeld, Comput. Phys. Rep. **1**, 389 (1984).
[16]P. M. Bellan, *Fundamentals of Plasma Physics* (Cambridge University Press, Cambridge, 2006), p. 609.
[17]E. Weibel, Am. J. Phys. **36**, 1130 (1968).